CHEMISTRY
A EUROPEAN JOURNAL

FULL PAPER

DOI: 10.1002/chem.201204199

Structure–Reactivity Relationships in the Hydrogenation of Carbon Dioxide with Ruthenium Complexes Bearing Pyridinylazolato Ligands

Keven Muller, Yu Sun, Andreas Heimermann, Fabian Menges, Gereon Niedner-Schatteburg,* Christoph van Wüllen,* and Werner R. Thiel*[a]

Abstract: Pyridinylazolato (N–N′) ruthenium(II) complexes of the type $[(N–N')RuCl(PMe_3)_3]$ have been obtained in high yields by treating the corresponding functionalised azolylpyridines with $[RuCl_2(PMe_3)_4]$ in the presence of a base. ^{15}N NMR spectroscopy was used to elucidate the electronic influence of the substituents attached to the azolyl ring. The findings are in agreement with slight differences in the bond lengths of the ruthenium complexes. Furthermore, the electronic nature of the azolate moiety modulates the catalytic activity of the ruthenium complexes in the hydrogenation of carbon dioxide under supercritical conditions and in the transfer hydrogenation of acetophenone. DFT calculations were performed to shed light on the mechanism of the hydrogenation of carbon dioxide and to clarify the impact of the electronic nature of the pyridinylazolate ligands.

Keywords: carbon dioxide · hydrogenation · nitrogen heterocycles · phosphanes · ruthenium

Introduction

To solve the problems of climate change and declining fossil resources, investigations into alternative carbon sources are of the utmost importance. For this purpose, carbon dioxide is worthy of consideration as an omnipresent, renewable and inexpensive C1 carbon source.[1] At about 146×10^6 tonnes per year, the production of urea is the most important industrial process based on carbon dioxide, followed by the synthesis of salicylic acid (Kolbe–Schmitt reaction) and the synthesis of poly(propylene carbonate).[2]

During the last decade, methods have been devised to transform carbon dioxide directly into organic molecules.[3] Although most effort has been focussed on the hydrogenation of this molecule, it should not be forgotten that dihydrogen is currently mainly generated from fossil sources. This may change in the future when cheap dihydrogen might become available from chemical or electrochemical water splitting or other benign processes.

In principle, a series of C1 products, such as formic acid and formates, formaldehyde, carbon monoxide, methanol or methane, are accessible from carbon dioxide,[4] although some of these reactions are thermodynamically unfavourable. Formic acid and formates are of special interest as hydrogen-storage compounds for several reasons: the hydrogen content of formic acid is quite high (approx. 4.3 wt%),[5] formic acid and formates are non-toxic liquids or solids that facilitate storage and transportation, and even simple palladium on charcoal catalyses the back-reaction to dihydrogen and carbon dioxide or carbonates. Last but not least, the dihydrogen used for the reduction of carbon dioxide is completely transferred into the formic acid/formate molecule, which is in contrast, for example, to the formation of methane from carbon dioxide in which two equivalents of dihydrogen end up in water. This makes formic acid interesting for hydrogen storage for fuel cells running small devices.

It is therefore not surprising that the hydrogenation of carbon dioxide has been investigated for more than two decades. The hydrogenation of carbon dioxide over nickel catalysts to yield methane (the Sabatier process), beneficially carried out with hydrogen from renewable resources, provides access to a molecule that is widely used as an energy source but also as a substrate in industry. Although heterogeneous copper, nickel and gold catalysts have mainly been considered to be capable of reducing carbon dioxide to carbon monoxide, methanol, methane or alkanes,[6] the formation of formic acid by heterogeneous catalysis has recently been reported. Fachinetti and co-workers described the formation of formic acid from carbon dioxide over a heterogeneous gold catalyst[7] and Ma and Zheng and their coworkers reported the use of heterogeneous $[Ru(OH)_3]$ and $[RuCl_2(PPh_3)]$, respectively, immobilised on MCM-41 to catalyse this reaction.[8] It is therefore not surprising that ruthenium compounds are the catalysts of choice in the homogeneous hydrogenation of carbon dioxide,[9] although some quite active rhodium and iridium compounds have also been reported.[10]

[a] Dipl. Chem. K. Muller, Dr. Y. Sun, A. Heimermann, F. Menges, G. Niedner-Schatteburg, C. van Wüllen, Prof. Dr. W. R. Thiel
Fachbereich Chemie, Technische Universität Kaiserslautern
Erwin-Schrödinger-Str. 52–54, 67663 Kaiserslautern (Germany)
Fax: (+49) 631 2054676
E-mail: thiel@chemie.uni-kl.de

Supporting information for this article is available on the WWW under http://dx.doi.org/10.1002/chem.201204199.

The pioneering concepts relating to the hydrogenation of carbon dioxide to formic acid and formates have been summarised in a series of reviews.[4,9,11] These results also inspired investigations into the catalytic reduction of carbon dioxide to methanol with silanes[12] and the development of catalysts for the splitting of formic acid into carbon dioxide and hydrogen.[13]

The formation of HCOOH from carbon dioxide and hydrogen is an endergonic reaction ($CO_2+H_2 \rightleftharpoons HCOOH$; $\Delta G_{273K}=32.9\ kJ\,mol^{-1}$).[14] Thus, bases are used to shift the chemical equilibrium to the product by the formation of formates. With the help of NEt_3, Inoue et al. succeeded in the first homogeneous hydrogenation of carbon dioxide catalysed by Wilkinson's catalyst,[15] which was further improved in the 1990s by Leitner and co-workers.[16] A landmark in this field was set by Noyori and co-workers, who used ruthenium(II) complexes such as $[RuCl_2(PMe_3)_4]$ or $[RuH_2(PMe_3)_4]$ in supercritical carbon dioxide.[17] Turn-over numbers (TONs) of up to 7200 could be reached due to the high solubility of H_2 in this solvent, and a four-fold increase in TON was achieved with $[RuCl(OAc)(PMe_3)_4]$.[18]

During the last decade iridium catalysts have received increasing interest in the hydrogenation of carbon dioxide. Between 2007 and 2011, a number of iridium catalysts were reported to exhibit TONs above 200000 in aqueous solution with KOH as the base,[19] which was surpassed by Nozaki and co-workers, who reported an iridium pincer complex reaching a TON of 3.5 million under similar conditions.[20] Fukuzumi and Fujita and their co-workers showed that this reaction is possible with iridium at ambient pressure and temperature.[21] In 2011, Milstein and co-workers reported a pincer-type dihydrido iron complex that showed good activity in the hydrogenation of carbon dioxide in the presence of NaOH.[22]

We have been interested in elucidating the subtle structure–reactivity relationships in catalysis for quite some time.[23] Pyrazole-based ligands have turned out to be ideal motifs for this purpose because the synthetic pathways leading to these ligands allow the introduction of electron-withdrawing and -donating substituents without changing the steric properties of the ligand. With a series of such ligands in hand, it is therefore possible to gain a deeper insight into the electronic influence of a ligand on the activity of the catalyst separate from steric considerations. Thus, we report herein the synthesis and characterisation of ruthenium catalysts of the type $[(N–N')RuCl(PMe_3)_3]$ and their performance in the hydrogenation of carbon dioxide.

Results and Discussion

Synthesis and characterisation of the ruthenium catalysts: The pyrazole-based ligands **1a–f** used for coordination to the ruthenium centre were accessed by established procedures following Claisen or Claisen-type condensations and subsequent ring closing with hydrazine (Scheme 1),[23a,b,e] whereas the triazolylpyridines **1h–j** were synthesised in a three-step procedure starting from 2-cyanopyridine.[24] Unsubstituted 2-(1,2,4-triazol-5-yl)pyridine (**1g**) was obtained by heating the intermediate picolinimidohydrazide at reflux in concentrated formic acid.[25]

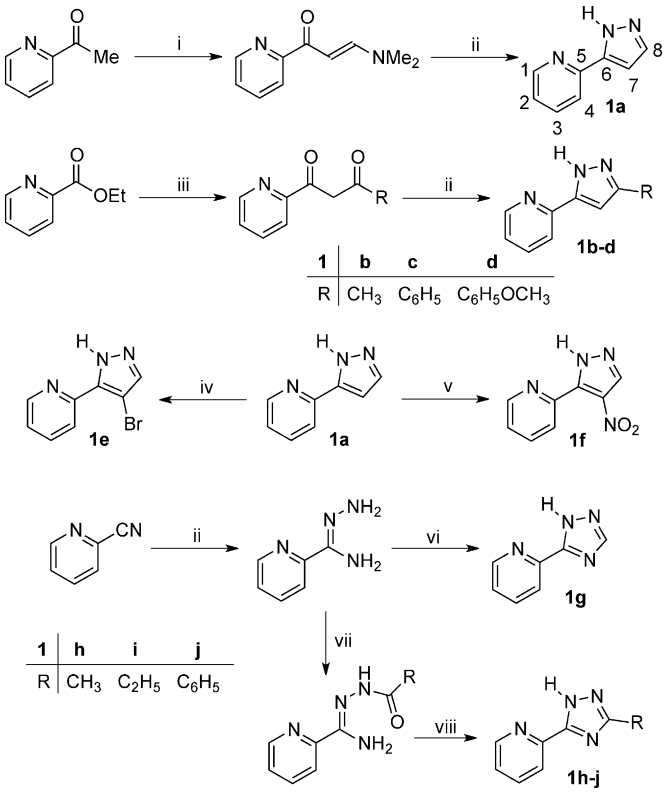

Scheme 1. Synthesis of the azolylpyridine ligands **1a–j**. Reagents and conditions: i) $HC(OMe)_2NMe_2$, reflux, 6 h; ii) N_2H_4, EtOH, reflux, 5 h; iii) MeC(O)R, NaOEt, 0–70 °C, 20 min; iv) Br_2, CH_3COOH, RT, 15 min; v) HNO_3, H_2SO_4, 0–90 °C, 4 h; vi) HCOOH, 0–25 °C, 1 h, then reflux, 4 h; vii) RCOCl, NaOH, DMF, 0–25 °C, 5 h; viii) > 200 °C, 5 min.

The direct synthesis of the corresponding ruthenium complexes by simple ligand exchange with the precursor $[RuCl_2(PMe_3)_4]$ gave only poor yields. Pyrazolylpyridines are known to undergo intramolecular hydrogen bonding between the N–H group of the pyrazole and the pyridine nitrogen atom,[23b,26] which will hinder coordination to the ruthenium(II) site. Therefore deprotonation of the ligands prior to the ligand-exchange reaction was performed with a slight excess of 1,8-diazabicycloundec-7-ene (DBU) as the base. Heating a solution of the deprotonated ligand in acetonitrile with $[RuCl_2(PMe_3)_4]$ at reflux gave quantitatively (by NMR spectroscopy) intense orange to red monochlorido complexes of the type $[(N–N')RuCl(PMe_3)_3]$ (**2a–f**, N–N′ = the pyridinylazolato ligand; Scheme 2). Slowly removing the solvent under vacuum directly led to the formation of single crystals, which in most cases were suitable for X-ray diffraction analysis (see below).

The coordination of the azolylpyridine ligands **1a–j** by ruthenium resulted in the expected changes in their ^1H NMR spectra. The resonance arising from the proton at the 1-position (for assignment see Scheme 1) of the pyridin-

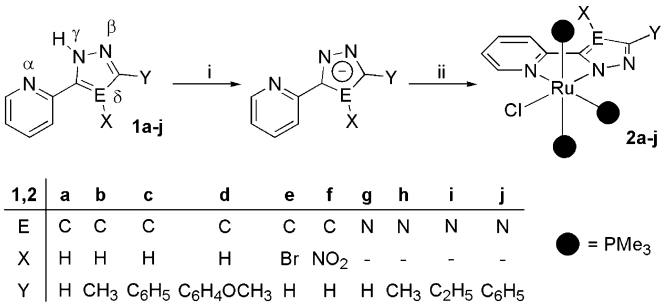

1,2	a	b	c	d	e	f	g	h	i	j
E	C	C	C	C	C	C	N	N	N	N
X	H	H	H	H	Br	NO_2	-	-	-	-
Y	H	CH_3	C_6H_5	$C_6H_4OCH_3$	H	H	H	CH_3	C_2H_5	C_6H_5

Scheme 2. Synthesis of the ruthenium complexes **2a–j**. Reagents and conditions: i) DBU, CH_3CN, 80 °C, 10 min; ii) $[RuCl_2(PMe_3)_4]$, CH_3CN, reflux, 1 h.

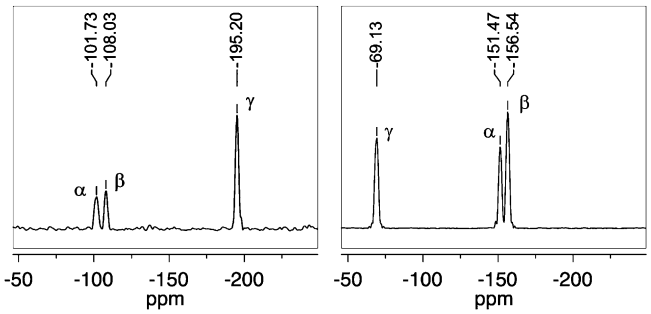

Figure 1. 1D ^{15}N HMBC NMR spectra of **1e** (left) and **2e** (right).

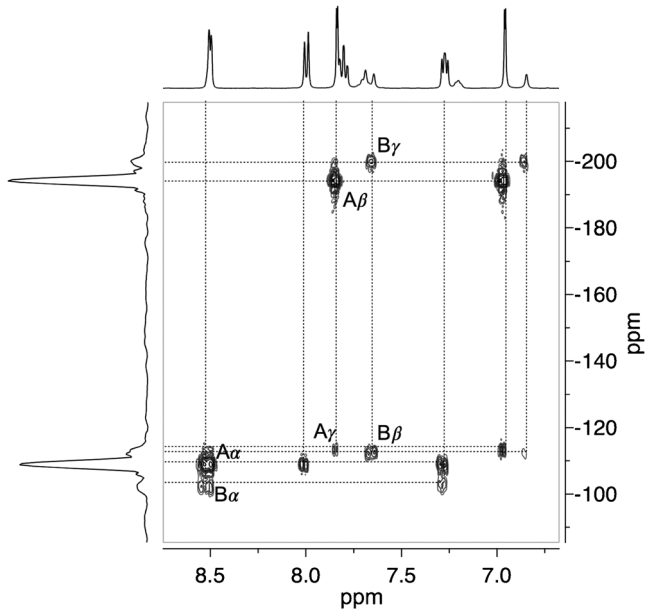

Figure 2. 2D ^{15}N HMBC NMR spectrum of **1a** (f_1: ^1H; f_2: ^{15}N).

yl ring shifts by 0.6–0.7 ppm to a lower field compared with the free ligand. All other ^1H NMR resonances are only slightly shifted to a higher field. In accord with a meridional arrangement of the three PMe_3 ligands, the ^{31}P NMR spectra show the typical AB_2 coupling pattern with a triplet for one equatorial PMe_3 moiety at 13–14 ppm and a doublet for the two chemically identical PMe_3 ligands in axial positions at about −2 to −5 ppm.

Although the influence of the azolylpyridine substitution pattern on the ^{31}P NMR chemical shifts is rather weak, strong effects were observed in the ^{15}N HMBC NMR experiments (HMBC = heteronuclear multiple bond correlation). The discussion here shall be limited to a few examples; an extended set of data is summarised in Table 1. The

Table 1. ^{15}N HMBC NMR data for selected ligands and ruthenium(II) complexes in $CDCl_3$.[a]

Compound	δ [ppm]			
	Nα	Nβ	Nγ	Nδ
1a, tautomer A	−109.29	−112.71	−194.44	–
1a, tautomer B	−102.17	−200.04	−114.13	–
1e	−101.73	−108.03	−195.20	–
1h	−102.82	−123.15	−189.84	−163.31
2a	−152.85	−159.38	−69.19	–
2c	−172.48	−145.09	−77.37	–
2e	−156.54	−151.47	−69.13	–
2f	−137.02	−149.09	−72.04	–
2g	−150.40	−158.13	−83.14	not obs.
2h	−151.35	−160.17	−84.56	not obs.

[a] For the atom numbering, see Scheme 2.

^{15}N HMBC NMR spectrum of ligand **1e** (Figure 1a) shows the three expected resonances for the nitrogen atom Nα (for the atom numbering see Scheme 2) of the pyridine ring at −101.73 ppm, which is close to the resonance at −108.03 ppm of the nitrogen atom Nβ at the 1-position of the pyrazole ring, and at −195.20 ppm for the pyrazole nitrogen atom Nγ at the 2-position of the pyrazole ring. The situation may become more complicated in some cases as a result of temperature-dependent tautomerism: in the ^{15}N HMBC NMR spectrum of ligand **1a** recorded at 229 K, for example, there are two tautomers visible in a ratio of approximately 4:1. The signals marked A in Figure 2 correspond to the thermodynamically most stable form in which the proton at the nitrogen atom at the 2-position of the pyrazole ring interacts with the nitrogen atom of the pyridine ring.[23b] The signals marked B correspond to the thermodynamically less stable tautomer in which the proton is located on the nitrogen at the 1-position of the pyrazole ring.

Coordination to the ruthenium(II) site leads to a considerable shift in the ^{15}N NMR resonances. For the ruthenium complex **2e** derived from ligand **1e**, the resonance of the pyrazole nitrogen atom Nγ at the 2-position is observed at −69.13 ppm (Figure 1b). The two other ^{15}N resonances are shifted upfield by around 100 ppm. This is a general finding for all the pyridinylpyrazolate complexes. For the triazolylpyrazolate complexes **2g–j**, the resonances of the two coordinating nitrogen atoms are detected at about −150 and −160 ppm. The nitrogen atom at the 2-position of the triazolate ring gives a peak at around −85 ppm, whereas the nitrogen atom at the 4-position was not observed.

In the IR spectra of the azolylpyridines the N–H stretching frequency appears between 3200 and 3100 cm^{-1}. This absorption is of course absent in the IR spectra of the ruthenium complexes. The absorptions of the PMe_3 methyl groups are typically observed at 2974 and 2910 cm^{-1}, and a very strong signal at 934 cm^{-1} can be assigned to a scissoring vibration of the methyl groups on the axially coordinated PMe_3 ligands.

To clarify the influence of the substituents at the azolyl units on catalyst stability independent of the influence of the solvent, some of the ruthenium pyrazolylpyridine complexes (**2a**, **2b**, **2e** and **2f**) were investigated by mass spectrometry (ESI–MS). There are two ways to generate monocationic species from the neutral precursors. First, a chlorido ligand can be removed leading to the 16-valence-electron cation $[(N–N')Ru(PMe_3)_3]^+$ ($[M-Cl]^+$). This would provide an open coordination site for catalysis in solution. Alternatively, an electron might be lost to give $[(N–N')RuCl(PMe_3)_3]^+$ ($[M]^+$). These processes may be accomplished by loss of PMe_3 and/or uptake of a molecule of acetonitrile (the solvent). As expected, loss of the chelating pyridylpyrazolate was not observed (see the Supporting Information for the corresponding spectra). The relative intensities of the different ionisation processes are presented in Table 2.

The modes by which the cationic species are formed differ with the substitution pattern of the ruthenium pyridylpyrazolate complexes. Compound **2f**, equipped with a strongly electron-withdrawing nitro group at the 4-position of the pyrazolate ring, mainly undergoes chloride loss followed by the addition of acetonitrile. However, a large number of ionic species are formed in the course of the ESI process as a result of oxidation: $[M]^+$ (15%), $[M-PMe_3+CH_3CN]^+$ (5%) and $[M-PMe_3]^+$ (1%). For compound **2e** with a bromo substituent at the same position, simple loss of the chlorido ligand is the dominant process. The uptake of acetonitrile after loss of the chlorido ligand ($[M-Cl+CH_3CN]^+$ (11%)) and oxidation are strongly suppressed ($[M]^+$ (0%) and $[M-PMe_3+CH_3CN]^+$ (8%)). The ESI-MS data for compounds **2a** and **2b** show that the cations obtained by dissociation of the chlorido ligand are quite stable because the tendency for the cation to take up acetonitrile is not as pronounced as for **2e**.

A number of the pyrazolyl- and triazolylpyridine ruthenium complexes gave crystals suitable for X-ray structure analysis. The molecular structures of compounds **2c–i** are presented in Figure 3 and selected bond lengths and angles are presented in Table 3. Directed by the different *trans* influences of the pyridine and pyrazolate/triazolate moieties, the complexes all adopt a distorted octahedral coordination environment with the three trimethylphosphane ligands oriented in a meridional arrangement and the chloride ligand located *trans* to the pyrazolate/triazolate donor. This is in agreement with the ^{31}P NMR data of the complexes. Depending on the donor strengths of the azolate and pyridine sites, the Ru–N2 distances are approximately 0.13 Å shorter than the Ru–N1 distances. There are slight differences in the bond lengths depending on the nature and substitution pattern of the azolate ring: the complexes containing triazolate moieties have longer Ru–N2 bonds than those containing pyrazolate rings and electron-donating substituents lead to a slight elongation of the Ru–N2 bond (in the pyrazolate series: $C_6H_4OMe > C_6H_5 > Br > NO_2$).

Table 2. Relative intensities[a] of the species observed in the ESI-MS spectra of the complexes **2a**, **2b**, **2e** and **2f**.

Species	Relative intensity [%]			
	2a	**2b**	**2e**	**2f**
$[M+CH_3CN]^+$	3	6	7	0
$[M-Cl+CH_3CN]^+$	5	5	11	65
$[M]^+$	0	0	0	15
$[M-Cl]^+$	79	76	67	9
$[M-PMe_3+CH_3CN]^+$	8	8	8	5
$[M-PMe_3]^+$	0	1	0	1
$[M-Cl-PMe_3]^+$	2	1	0	1

[a] Missing percentages are due to unassignable species with relative intensities of < 1%.

Catalysis: The hydrogenation of carbon dioxide under supercritical conditions was performed in a stainless-steel auto-

Table 3. Characteristic bond lengths [Å] and angles [°] for the ruthenium(II) complexes **2c–i**.

	2c[a]	**2d**	**2e**[a]	**2f**[a]	**2g**	**2h**[a]	**2i**
bond lengths [Å]							
Ru1–Cl1	2.4547(8)	2.4534(7)	2.4639(5)	2.4387(6)	2.4427(4)	2.4419(7)	2.4574(7)
Ru1–P1	2.3372(8)	2.3451(8)	2.3491(5)	2.3553(7)	2.3565(5)	2.3449(8)	2.3451(8)
Ru1–P2	2.2776(8)	2.2838(8)	2.2892(5)	2.2840(6)	2.2748(5)	2.2807(8)	2.2787(9)
Ru1–P3	2.3543(9)	2.3419(7)	2.3425(5)	2.3422(6)	2.3533(5)	2.3464(7)	2.3453(8)
Ru1–N1	2.171(3)	2.155(2)	2.1497(14)	2.1386(19)	2.1543(16)	2.168(2)	2.163(2)
Ru1–N2	2.031(3)	2.039(2)	2.0218(15)	2.023(2)	2.0394(16)	2.046(2)	2.034(3)
bond angles [°]							
Cl1-Ru1-P1	86.73(3)	86.75(3)	87.28(2)	86.98(2)	88.63(2)	85.65(3)	86.35(2)
Cl1-Ru1-P2	97.19(3)	96.00(3)	95.67(2)	95.57(2)	94.71(2)	97.47(3)	95.53(3)
Cl1-Ru1-P3	84.78(3)	87.46(2)	87.64(2)	87.42(2)	87.42(2)	86.60(2)	87.74(2)
Cl1-Ru1-N1	94.00(7)	91.99(6)	93.41(4)	93.13(5)	93.17(4)	91.18(7)	93.53(5)
Cl1-Ru1-N2	171.07(7)	169.28(6)	170.81(4)	169.60(6)	170.28(5)	168.68(7)	170.13(7)
P1-Ru1-P2	93.21(3)	92.08(3)	93.74(2)	93.55(2)	94.50(2)	92.01(3)	92.59(3)
P1-Ru1-P3	169.90(3)	172.56(3)	171.64(2)	172.59(2)	172.03(2)	171.19(3)	171.71(3)
P1-Ru1-N1	87.75(7)	87.29(6)	86.88(4)	87.34(5)	87.68(4)	87.73(7)	86.46(6)
P1-Ru1-N2	92.84(8)	94.51(6)	91.71(4)	91.60(6)	91.88(5)	94.28(7)	92.13(7)
P2-Ru1-P3	93.28(3)	93.17(3)	93.36(2)	91.82(2)	92.72(2)	93.15(3)	93.76(3)
P2-Ru1-N1	168.80(7)	171.94(6)	170.92(4)	171.29(5)	171.87(4)	171.31(7)	170.81(6)
P2-Ru1-N2	91.74(7)	94.59(6)	93.52(4)	94.81(6)	94.93(5)	93.85(7)	94.28(7)
P3-Ru1-N1	87.39(7)	88.25(6)	86.80(4)	88.12(5)	85.64(4)	88.24(7)	88.11(5)
P3-Ru1-N2	94.69(8)	90.33(6)	92.24(4)	93.03(6)	90.86(5)	92.50(7)	92.71(8)
N1-Ru1-N2	77.07(10)	77.45(8)	77.40(6)	76.50(7)	77.15(6)	77.51(10)	76.64(8)

[a] There are two independent molecules in the unit cell, the data of only one is presented here.

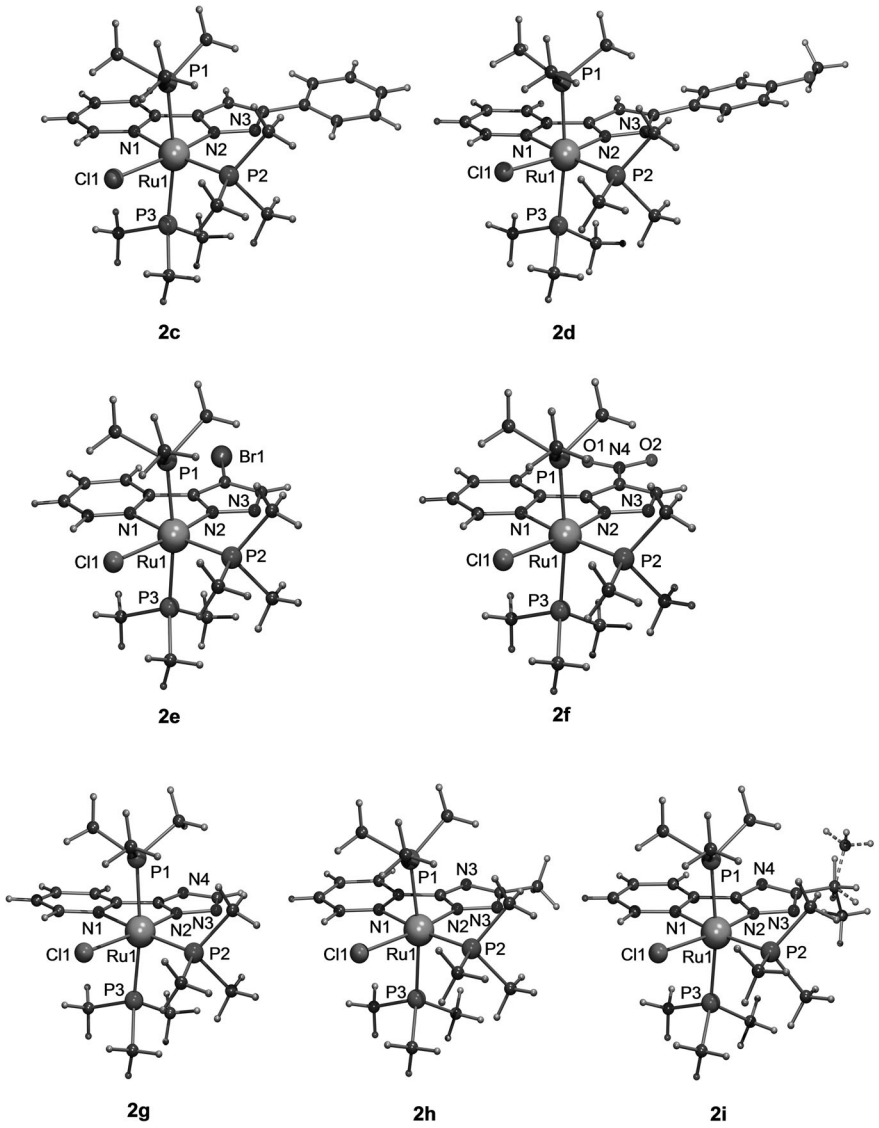

Figure 3. Molecular structures of the ruthenium(II) complexes **2c–i** in the solid state. Two crystallographically independent molecules were found in the unit cells of **2c**, **2e**, **2f** and **2h**, only one of which is shown here. The ethyl group of compound **2i** is disordered over two positions.

clave suitable for high pressures. To avoid the need for a compressor to attain the desired carbon dioxide pressure, a method using solid carbon dioxide was established and is described in the experimental part of this paper. Often an amine base is required to stabilise the generated formic acid. The resulting salts can be cleaved at high temperatures allowing the reuse of the amine after distillation of the raw product.[27] Under the given reaction conditions, 1,8-diazabicyclo[5.4.0]undec-7-ene (DBU) gave the best performance compared with other amine bases, such as the frequently used triethylamine.[18] It is well established in carbon dioxide hydrogenation catalysis that sub-stoichiometric amounts of a proton source promote the production of formic acid. C_6F_5OH, with a pK_a on the aqueous scale below that of the protonated amine, was reported to provide the best results.[18] Therefore we chose this additive.

Table 4. Catalyst screening for the hydrogenation of carbon dioxide.[a]

	Catalyst	n(HCOOH) [mmol]	n(HCOOH)/n(DBU)	TON	TOF [h^{-1}]
1	**2a**	44	0.67	4300	1080
2	**2b**	34	0.51	3200	800
3	**2c**	34	0.50	2980	740
4	**2d**	30	0.46	3000	750
5	**2e**	40	0.60	4000	1000
6	**2f**	41	0.63	4200	1050
7	**2g**	49	0.74	4800	1200
8	**2h**	38	0.57	3700	920
9	**2i**	45	0.68	4450	1110
10	**2j**	40	0.61	3670	920
11	$[RuCl_2(PPh_3)_3]$	18	0.27	1520	380
12	$[RuCl_2(PMe_3)_4]$	77	1.17	7600	1900

[a] Reagents and conditions: CO_2 (20 g), $p(H_2, 293\ K) = 70$ bar, p_{total} (100 °C) = 170 bar, C_6F_5OH (20 mg), catalyst (0.01 mmol), DBU (65 mmol), $T = 100$ °C, $t = 4$ h.

The TONs and TOFs of the complexes studied in this work are presented in Table 4. Compared with catalyst **2a** (Table 4, entry 1) with a completely unsubstituted ligand, catalyst **2b**, which bears an electron-donating methyl substituent (+I effect) at the 5-position of the pyrazole ring, is clearly less active (Table 4, entry 2). The introduction of substituents with a π system in conjugation with the pyrazole moiety further lowers the catalytic activity (**2c** and **2d**, Table 4, entries 3 and 4). It was therefore expected that electron-withdrawing groups would lead to a better performance. However, this is not true for substituents at the 4-position: the catalysts **2e** and **2f** (Table 4, entries 5 and 6), which carry electron-withdrawing substituents at this site, show slightly lower activities than **2a**. The trend is similar for the triazole series but the performances of ruthenium complexes with the same substitution pattern as the pyrazole series are generally higher (compare catalysts **2a–c** with catalysts **2g**, **2h** and **2j**). It seems that ligands equipped with an electron-withdrawing substituent show better catalytic activity. For comparison, the phosphane complexes $[RuCl_2$-

$(PPh_3)_3$] and [$RuCl_2(PMe_3)_4$] were also investigated. Although the activity of the triphenylphosphane complex is reduced by a factor of about 2.8 compared with **2a**, the trimethylphosphane derivative shows an activity increased by a factor of 1.7. We are currently carrying out quantum chemical calculations that might help to differentiate between the electronic and steric influences of the substituents on the nitrogen donor and the phosphanes.

To gain more experimental data on the electronic effects of the pyridinylazolate ligands, the catalysts were also tested in the transfer hydrogenation of acetophenone with 2-propanol as the hydrogen source (Table 5). The complexes with

Table 5. Catalyst screening for the transfer hydrogenation of acetophenone with 2-propanol.[a]

	Catalyst	Yield [%]	
		After 4 h	After 24 h
1	**2a**	18	48
2	**2b**	1	4
3	**2c**	19	84
4	**2d**	41	82
5	**2e**	4	23
6	**2f**	11	57
7	**2g**	16	48
8	**2h**	21	54
9	**2i**	23	56
10	**2j**	32	69
11	[$RuCl_2(PPh_3)_3$]	54	86
12	[$RuCl_2(PMe_3)_4$]	44	99

[a] Reagents and conditions: 2-propanol (15 mL), catalyst (0.01 mmol), *t*BuOK (0.25 mmol), acetophenone (5.0 mmol), $T = 80\,°C$.

substituents possessing an aromatic substituent at the 5-position (**2c** and **2d** for the pyrazole series and **2j** for the triazole series) gave the best yields after 24 h. For comparison, the brominated and nitrated pyrazole-based systems **2e** and **2f** showed lower activity, as did the methylated species **2b**, which yielded almost no product.

Quantum chemical calculations: To gain a better understanding of the electronic effects of the pyrazole-based ligands on the catalytic performance of the ruthenium complexes, quantum chemical calculations were carried out. There is broad agreement in the literature that hydrido ruthenium complexes, either used directly or formed in situ, are the active species in the hydrogenation of carbon dioxide to formic acid and its derivatives.[20,28] A complete calculation of the mechanism based on the [$Ru(H)_2(PMe_3)_3$] catalyst was carried out by Sakaki and co-workers.[29] They found that the insertion of carbon dioxide into the Ru–H bond is the rate-determining step. The activation barrier for this process decreases with increasing polarity of the solvent. Our DFT study allowed elucidation of the mechanism of hydrogenation for four of the hydrido ruthenium catalysts (**2a**, **2e**, **2f** and **2g**) bearing different pyridinylazolate ligands. The energetics of different substitution patterns are presented below and details concerning the calculations are summarised in the Experimental Section. The atom coordinates and energies for all the calculated structures are presented in the Supporting Information. Note that the high partial pressures (concentrations) of carbon dioxide and dihydrogen were taken into account in the calculations of the free enthalpies (Gibbs free energies).

The hydrogenation cycle, shown in Scheme 3 exemplarily for catalyst **2a**, starts with the 16-valence-electron complex [(N–N′)Ru(H)$(PMe_3)_2$] (**A**). Owing to the weaker *trans* in-

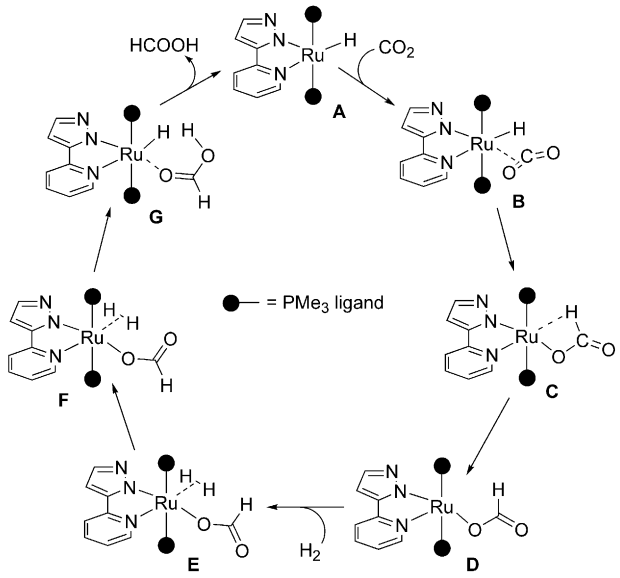

Scheme 3. Proposed mechanism for the hydrogenation of carbon dioxide with (pyridinylazolato)ruthenium catalysts. The transition states have been omitted for clarity.

fluence of pyridine versus azolato ligands, the hydrido ligand is located *trans* to the pyridine unit. The energies calculated for the analogous reaction mechanism starting with the hydrido ligand *trans* to the azolato ligand are systematically higher than the energies determined for the structures shown in Scheme 3. At several points of the mechanism, the site of reactivity could change from *trans* to pyridine to *trans* to the azolato unit and vice versa. This behaviour was calculated for a series of steps for catalyst **2e**; it was found that the barriers to such isomerisation reactions are quite high (see the Supporting Information). Figure 4 shows the calculated free enthalpies for all intermediates and transition states generated from [(N–N′)Ru(H)$(PMe_3)_2$] (**A**) bearing the hydrido ligand *trans* to the pyridine unit. Depending on the nature of the pyridylazolato ligand, the coordination of carbon dioxide is either slightly endergonic, for ligands **2e** and **2f** bearing an electron-withdrawing group, or exergonic, for ligands **2a** and **2g**. Carbon dioxide coordinates to the ruthenium(II) site in intermediate **B** in a η^2-coordination mode and adopts a bent structure with an O–C–O angle of around 140°. With an activation barrier of around 25–30 kJ mol^{-1}, the hydrido ligand is transferred to the carbon atom via a four-membered-ring transition state leading to an O,H-coordinated formato ligand (**C**). Although the free en-

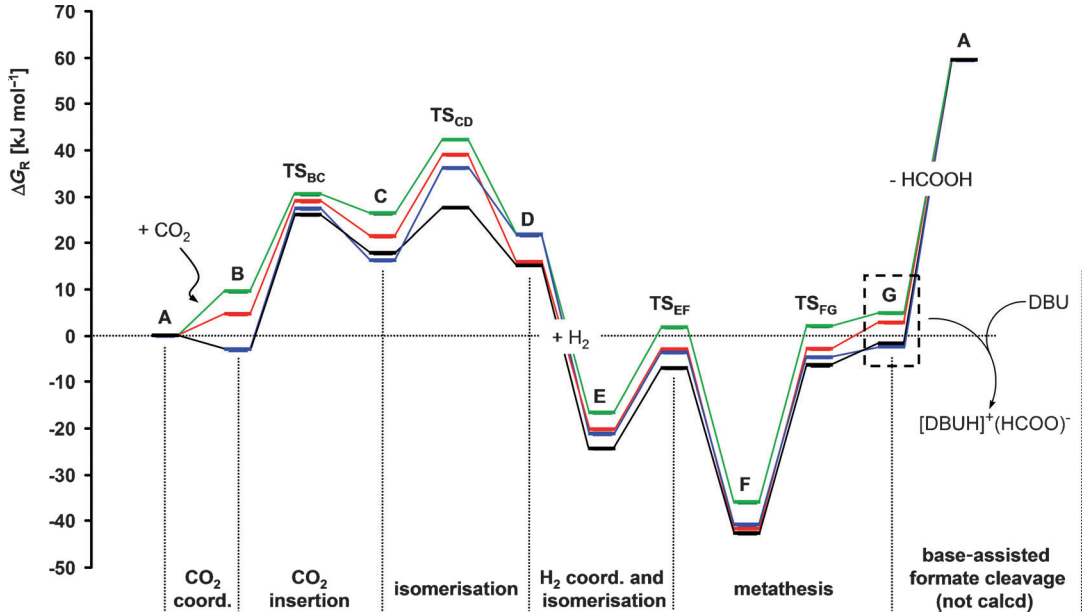

Figure 4. Calculated profiles of the free reaction enthalpies for the hydrogenation of carbon dioxide with the catalysts **2a** (black), **2e** (red), **2f** (green) and **2g** (blue). For the structures **A**–**G**, see Scheme 3.

thalpies of the transition state $\mathbf{TS_{BC}}$ are largely independent of the substitution pattern of the azolate moiety, there is a clear influence on the structure **C**. This fact is even more pronounced in the subsequent transition state $\mathbf{TS_{CD}}$ for the opening up of a free coordination site for the incoming dihydrogen; the ruthenium centre changes from an 18- to a 16-valence-electron state. $\mathbf{TS_{CD}}$ is the point of highest enthalpy in the whole catalytic cycle (for the final step, see below) for all ligand substitution patterns calculated. The absolute barriers differ by about 15 kJ mol^{-1}, although the differences in the barriers relative to structure **C** are less pronounced. The overall reaction **C**→**D** is slightly exergonic except for catalyst **2g**, the only system bearing a pyridinyltriazolato ligand. This step is followed by the strongly exergonic addition of dihydrogen (ca. −40 kJ mol^{-1}), which leads to the 18-valence-electron system **E**. For the subsequent transfer of a hydrogen atom to the formate anion, this ligand has to undergo a rotation around the C–O bond to bring the oxygen atom into close proximity to the dihydrogen ligand. The rotation is hindered by a barrier of about 17 kJ mol^{-1}, almost independent of the nature of the pyridinylazolato ligand, and the final product **F** is stabilised by around 20 kJ mol^{-1} with respect to the starting structure **E**. There is again almost no influence of the ligand substitution pattern on the reaction enthalpy $\Delta G_R(\mathbf{E})-\Delta G_R(\mathbf{F})$. The following transfer of a hydrogen atom proceeds via a late six-membered-ring transition state. This reaction is endergonic by about 45 kJ mol^{-1} and the reaction barrier is around 38 kJ mol^{-1} and thus lower than the free enthalpy of the reaction. This is due to the fact that the electronic energies and not the free enthalpies were optimised, which excludes entropic effects. The final dissociation of formic acid from the intermediate **G** to regenerate the hydrido complex **A** is endergonic by about 55–65 kJ mol^{-1}. In this step, ligands equipped with an electron-withdrawing substituent have a lower barrier. The overall free enthalpy of the reaction is around +55 kJ mol^{-1}. In practical applications, an ammonium formate is formed instead by addition of a base (here DBU). This lowers the total enthalpy considerably and makes the whole reaction sequence thermoneutral or slightly exothermic.

According to the DFT calculations, the detachment of the formate hydrogen atom from the ruthenium site leading to a 16-valence-electron intermediate is the rate-determining step. The calculated barriers show a clear dependence on the ligand structure ($\Delta G_R(\mathbf{TS_{CD}})$: **2a**<**2e**<**2f**<**2g**). In the pyrazolylpyridine series (**2a**, **2e**, **2f**), the barrier rises with increasing electron-withdrawing effect of the substituent (N < Br < NO_2). This is not reflected in the observed differences in catalytic activity. The pyridinyltriazolato catalyst **2g** in reality shows a performance even better than **2a** even though its barrier for $\mathbf{TS_{CD}}$ is higher. The structural effects observed in the catalytic hydrogenation of carbon dioxide must therefore not only be related to the electronic impact of the substituents but also be due to further interactions with the solvent and/or additives present in the catalytic reaction. As mentioned above, the dissociation of the formate from the ruthenium site leading to $DBUH^+(HCOO^-)$ is a crucial step in which the interaction of the bulky DBU with intermediate **G** is dependent on the size of the chelating ligand.

Conclusion

Azolylpyridines coordinate to $[RuCl_2(PMe_3)_4]$ in the presence of a base to give the corresponding pyridinylazolato complexes $[(N–N')RuCl(PMe_3)_3]$ in which the chloride ligand is *trans* to the azolato site. The ligands and ruthenium complexes were completely characterised by a number of techniques, including ^{15}N NMR spectroscopy. ESI mass spectrometry showed that the ruthenium complexes follow different ionisation and fragmentation pathways depending on the substitution pattern of the azolato moiety. These differences were also found in the catalytic hydrogenation of carbon dioxide to formates under supercritical conditions. Compared with a standard system such as $[RuCl_2(PMe)_4]$, the ruthenium complexes developed in this work showed good activities that varied with the substituents on the chelating nitrogen ligand. In general, the unsubstituted ligands gave the best performances with the triazolato system being even more active than the pyrazolato complex. DFT calculations performed to ascertain the reaction mechanism allowed the electronic influence of the substituents to be clarified; the results showed good correlation with the catalytic activities observed for the pyridinylpyrazolato series.

Experimental Section

General: All manipulations were carried out under an atmosphere of purified argon by using standard Schlenk techniques. Elemental analyses were carried out at the Department of Chemistry, TU Kaiserslautern. IR spectra were recorded with a Perkin-Elmer Spectrum 100 FT-UATR-IR spectrometer equipped with a Diamond/ZnSe plate. NMR spectra were recorded with Bruker DPX 400 and Avance 600 spectrometers. ESI-MS spectra were recorded on a modified Bruker amaZonSL mass spectrometer. The spectroscopic data of all compounds synthesised in this work are reported in the Supporting Information. The pyridylpyrazole and -triazole based ligands were prepared following previous reports in the literature.[23a–c,24,25] Ligand **1d** was synthesised following the same process as used for **1c**. The ruthenium precursors $[RuCl_2(PPh_3)_3]$ and $[RuCl_2(PMe_3)_4]$ were obtained from $RuCl_3$ (Strem) according to literature procedures.[30,31]

General procedure for the synthesis of the ruthenium complexes 2a–j: 1,8-Diazabicycloundec-7-ene (DBU; 60 μL) was added to a solution of the appropriate pyrazolyl- or triazolylpyridine **1a–j** (0.4 mmol) in acetonitrile (10 mL) and the mixture was heated at reflux for 10 min. After cooling to room temperature, $[RuCl_2(PMe_3)_4]$ (190.4 mg, 0.4 mmol) was added and the mixture was heated at reflux for 1 h . Then the solvent was reduced to around 3 mL. After several hours, yellow to orange crystals of the desired ruthenium complexes were separated from the liquid and recrystallised from acetonitrile. All yields given below are for the recrystallised samples. The conversions were generally almost quantitative, however, the $DBUH^+Cl^-$ salts had to be separated.

Chlorido[5-(pyridin-2-yl)pyrazolato]tris(trimethylphosphine)ruthenium(II) (2a): Yield: 23%. Elemental analysis calcd (%) for $C_{17}H_{33}ClN_3P_3Ru$: C 40.12, H 6.54, N 8.26; found: C 40.02, H 6.43, N 8.30.

Chlorido[3-methyl-5-(pyridin-2-yl)pyrazolato]tris(trimethylphosphine)ruthenium(II) (2b): Yield: 22%. Elemental analysis calcd (%) for $C_{18}H_{35}ClN_3P_3Ru\cdot(CH_3CN)$: C 42.59, H 6.79, N 9.93; found: C 42.95, H 6.67, N 9.15.

Chlorido[3-phenyl-5-(pyridin-2-yl)pyrazolato]tris(trimethylphosphine)ruthenium(II) (2c): Yield: 32%. Elemental analysis calcd (%) for $C_{23}H_{37}ClN_3P_3Ru\cdot(CH_3CN)$: C 47.96, H 6.44, N 8.95; found: C 48.05, H 6.60, N 9.08.

Chlorido[3-(4-methoxyphenyl)-5-(pyridin-2-yl)pyrazolato]tris(trimethylphosphine)ruthenium(II) (2d): Yield: 30%. Elemental analysis calcd (%) for $C_{24}H_{39}ClN_3OP_3Ru$: C 46.87, H 6.39, N 6.83; found: C 46.70, H 6.28, N 6.73.

[4-Bromo-5-(pyridin-2-yl)pyrazolato]tris(trimethylphosphine)chloridoruthenium(II) (2e): Yield: 65%. Elemental analysis calcd (%) for $C_{17}H_{32}BrClN_3P_3Ru$: C 34.74, H 5.49, N 7.15; found: C 34.89, H 5.64, N 7.40.

Chlorido[4-nitro-5-(pyridin-2-yl)pyrazolato]tris(trimethylphosphine)ruthenium(II) (2f): Yield: 53%. Elemental analysis calcd (%) for $C_{17}H_{32}ClN_4O_2P_3Ru$: C 36.86, H 5.82, N 10.11; found: C 36.87, H 5.95, N 10.22.

Chlorido[5-(pyridin-2-yl)-1,2,4-triazolato]tris(trimethylphosphine)ruthenium(II) (2g): Yield: 37%. Elemental analysis calcd (%) for $C_{16}H_{32}ClN_4P_3Ru$: C 37.69, H 6.33, N 10.99; found: C 37.60, H 6.20, N 11.10.

Chlorido[3-methyl-5-(pyridin-2-yl)-1,2,4-triazolato]tris(trimethylphosphine)ruthenium(II) (2h): Yield: 39%. Elemental analysis calcd (%) for $C_{17}H_{34}ClN_4P_3Ru$: C 38.97, H 6.54, N 10.69; found: C 38.54, H 6.79, N 10.81.

Chlorido[3-ethyl-5-(pyridin-2-yl)-1,2,4-triazolato]tris(trimethylphosphine)ruthenium(II) (2i): Yield: 41%. Elemental analysis calcd (%) for $C_{18}H_{36}ClN_4P_3Ru$: C 40.19, H 6.75, N 10.41; found: C 40.08, H 6.66, N 10.34.

Chlorido[3-phenyl-5-(pyridin-2-yl)-1,2,4-triazolato]tris(trimethylphosphine)ruthenium(II) (2j): Yield: 24%. Elemental analysis calcd (%) for $C_{22}H_{36}ClN_4P_3Ru\cdot(CH_3CN)$: C 45.97, H 6.27, N 11.17; found: C 46.10, H 6.20, N 11.30.

Catalytic hydrogenation of carbon dioxide: The reactions were carried out in a stainless-steel autoclave (100 mL, Berghoff) suitable for pressures of up to 200 bar and equipped with a Teflon lining and an internal thermometer. DBU (10 g, 65 mmol), pentafluorophenol (20 mg, 0.14 mmol), dry, solid carbon dioxide (20 g) and the catalyst (0.01 mmol) were introduced into the autoclave, which was closed and pressurised with hydrogen (70 bar). Then the autoclave was placed in a preheated aluminium block. After 15 min of heating the required inner temperature of 100 °C and an overall pressure of 170 bar were reached and maintained for 4 h. The mixture was constantly stirred at 300 rpm. Then the autoclave was rapidly cooled to 5 °C in an ice bath, depressurised, opened and the reaction mixture analysed by ^1H NMR spectroscopy.

Catalytic transfer hydrogenation of acetophenone with 2-propanol: These reactions were carried out in a two-necked flask (50 mL) equipped with a reflux condenser and a Quickfit septum adapter. In this flask, the catalyst (0.01 mmol) was dissolved in 2-propanol (15 mL) and heated to 80 °C. KO*t*Bu (26.8 mg, 0.25 mmol) and acetophenone (0.6 g, 5.0 mmol) were then added to the mixture. Samples were taken every hour with a PE syringe and analysed by GC-MS.

ESI-MS: Sample solutions at concentrations of about 10^{-3} M were prepared under oxygen-free conditions in LC-MS-grade acetonitrile and stored at room temperature for some time to allow equilibration. The ion source was used in the positive electrospray ionisation mode. A scan speed of 32500 $m/z\,s^{-1}$ was used in ultra-scan mode (0.3 FWHM/m/z) and the scan range was at least 70–800 m/z. Sample solutions were continuously infused into the ESI chamber by means of a syringe pump at a flow rate of 2 $\mu L\,min^{-1}$. Nitrogen was used as drying gas at a flow rate of 3.0 $L\,min^{-1}$ at 220 °C. The solutions were sprayed at a nebuliser pressure of 4 psi (280 mbar) and the electrospray needle was held at 4.5 kV. Instruments were controlled with the BrukerTrapControl 7.0 software and data analysis was performed by using the Bruker Data Analysis 4.0 software.

X-ray structure analyses: Crystal data and refinement parameters for the ruthenium(II) complexes **2c–i** are presented in Table 6. The structures were solved by direct methods (SIR92[32]), completed by subsequent difference Fourier syntheses and refined by full-matrix least-squares procedures.[33] Semi-empirical absorption corrections (Multiscan) were carried

Table 6. Crystallographic data and parameters for data collection and refinement.

	2c	**2d**	**2e**	**2f**	**2g**	**2h**	**2i**
empir. formula	$C_{23}H_{37}ClN_3P_3Ru$	$C_{24}H_{39}ClN_3OP_3Ru$	$C_{17}H_{32}BrClN_3P_3Ru$	$C_{17}H_{32}ClN_4O_2P_3Ru$	$C_{16}H_{32}ClN_4P_3Ru$	$C_{17}H_{34}ClN_4P_3Ru$	$C_{18}H_{36}ClN_4P_3Ru$
M_r	584.99	615.01	587.80	553.90	509.89	523.91	537.94
crystal size [mm]	0.47×0.19×0.17	0.25×0.23×0.18	0.19×0.17×0.16	0.39×0.16×0.16	0.22×0.14×0.13	0.27×0.05×0.04	0.44×0.16×0.14
T [K]	150(2)	150(2)	150(2)	150(2)	150(2)	150(2)	150(2)
λ [Å]	1.54184	1.54184	0.71073	1.54184	1.54184	1.54184	1.54184
crystal system	triclinic	orthorhombic	triclinic	orthorhombic	orthorhombic	orthorhombic	monoclinic
space group	$P\bar{1}$	$P2_12_12_1$	$P\bar{1}$	$Pca2_1$	$Pbcn$	$Pca2_1$	$P2_1/c$
a [Å]	9.0227(3)	10.7125(1)	11.3465(3)	18.4387(2)	22.8818(1)	18.7398(2)	9.0284(1)
b [Å]	18.3572(6)	11.4555(1)	15.2651(4)	8.5206(1)	13.1475(1)	8.6339(1)	11.2453(2)
c [Å]	18.4391(6)	23.6612(3)	15.8486(4)	30.7663(3)	15.0458(1)	29.7087(3)	24.5818(4)
α [°]	103.315(3)	90	108.613(2)	90	90	90	90
β [°]	103.116(3)	90	105.962(2)	90	90	90	94.271(1)
γ [°]	103.215(3)	90	98.240(2)	90	90	90	90
V [Å^3]	2764.44(18)	2903.63(5)	2419.40(11)	4866.66(9)	4526.35(5)	4806.80(9)	2488.79(7)
Z	4	4	4	8	8	8	4
$\rho_{calcd.}$ [g cm^{-3}]	1.406	1.407	1.614	1.522	1.496	1.448	1.436
μ [mm^{-1}]	7.233	6.941	2.616	8.313	8.754	8.259	7.990
θ range [°]	3.06–62.68	3.74–62.64	2.70–32.56	4.80–62.66	3.86–62.64	2.97–62.66	3.61–62.64
reflns coll.	21155	20995	28909	39369	32904	35767	20341
indep. reflns	8820 [R_{int}=0.0314]	4606 [R_{int}=0.0293]	15667 [R_{int}=0.0243]	7649 [R_{int}=0.0283]	3617 [R_{int}=0.0309]	7394 [R_{int}=0.0340]	3987 [R_{int}=0.0250]
data/restr./param.	8820/0/577	4606/0/308	15567/0/487	7649/1/524	3617/0/236	7394/1/490	3987/3/265
final R indices $[I>2\sigma(I)]$[a]	0.0320, 0.0874	0.0205, 0.0494	0.0238, 0.0430	0.0170, 0.0441	0.0199, 0.0519	0.0184, 0.0427	0.0270, 0.0674
R indices (all data)	0.0350, 0.0890	0.0212, 0.0497	0.0384, 0.0441	0.0172, 0.0441	0.0207, 0.0524	0.0191, 0.0429	0.0284, 0.0681
GooF[b]	1.058	1.038	0.875	1.064	1.120	1.009	1.042
Flack parameter	–	0.009(7)	–	0.270(4)	0.00079(2)	0.569(5)	–
$\Delta\rho_{max}/_{min}$ [e Å^{-3}]	0.989/−0.742	0.166/−0.398	0.726/−0.670	0.383/−0.360	0.387/−0.453	0.943/−0.259	0.817/−0.756

[a] $R1=\Sigma||F_o|-|F_c||/\Sigma|F_o|$, $wR2=[\Sigma w(F_o^2-F_c^2)^2/\Sigma wF_o^2]^{1/2}$. [b] $GooF=[\Sigma w(F_o^2-F_c^2)^2/(n-p)]^{1/2}$.

out.[34] All non-hydrogen atoms were refined by using anisotropic displacement parameters. All hydrogen atoms were placed in calculated positions and refined by using a riding model.

CCDC-930861 (**2c**), CCDC-930862 (**2d**), CCDC-930863 (**2e**), CCDC-930864 (**2f**), CCDC-930865 (**2g**), and CCDC-930866 (**2h**), CCDC-930867 (**2i**) contain the supplementary crystallographic data for this paper. These data can be obtained free of charge from The Cambridge Crystallographic Data Centre via www.ccdc.cam.ac.uk/data_request/cif.

Quantum chemical calculations: All DFT calculations were performed with the B3LYP functional[35] with the TZVP basis set[36] for all atoms except ruthenium, for which a scalar relativistic effective core potential replacing 28 core electrons[37] was used together with a def-TZVP[38] valence basis set. Geometry optimisations for gas-phase species were performed with a combination of TURBOMOLE[39] and the Gaussian 03 program package[40] (by using the EXTERNAL interface of the latter) starting from the X-ray structures of the precatalysts. All minima and transition states were characterised by frequency calculations, transition states having exactly one negative Hessian eigenvalue. Intrinsic reaction coordinate (IRC) calculations were carried out to verify that the transition states really connect the two minima with which they are associated. In a second series of calculations, all the minima and transition states found so far were reoptimised by using the Gaussian 09[41] program package and solvent effects were also taken into account by using the COSMO[42] model with a dielectric constant $\varepsilon=1.3$ used for supercritical carbon dioxide, taken from Monte–Carlo molecular simulations.[43] The Gibbs free energies were calculated by using the Gaussian 09 package for all species in the catalytic cycle, as well as for dihydrogen and carbon dioxide, by using the harmonic approximation for the vibrational part, the rigid rotor approximation for the rotational part and the free particle model for the translational part of the partition function. A temperature of 373 K and a standard partial pressure of about 1 bar (1 atm) were used for ruthenium-containing species in the catalytic cycle. The concentrations of dihydrogen and carbon dioxide were much higher under the reaction conditions, which significantly influences the Gibbs free-energy differences for the corresponding association steps. Therefore a much higher partial pressure (estimated for the reaction conditions: 70 bar for dihydrogen, 100 bar for carbon dioxide) was used to calculate the Gibbs free energies for these two compounds.

Acknowledgements

The authors thank the Deutsche Forschungsgemeinschaft (ERA Chemistry and SFB/TRR 88) and the National Research Fund (FNR), Luxembourg, for financial support of this work.

[1] *Carbon Dioxide as Chemical Feedstock* (Ed.: M. Aresta), Wiley-VCH, Weinheim, **2010**.
[2] A. Bazzanella, D. Krämer, M. Peters, *Nachr. Chem.* **2010**, *58*, 1226–1230.
[3] T. Sakakura, J.-C. Choi, H. Yasuda, *Chem. Rev.* **2007**, *107*, 2365–2387.
[4] P. G. Jessop, T. Ikariya, R. Noyori, *Chem. Rev.* **1995**, *95*, 259–272.
[5] a) F. Joó, *ChemSusChem* **2008**, *1*, 805–808; b) S. Enthaler, J. von Langermann, T. Schmidt, *Energy Environ. Sci.* **2010**, *3*, 1207–1217; c) B. Loges, A. Boddien, F. Gärtner, H. Junge, M. Beller, *Top. Catal.* **2010**, *53*, 902–914; d) M. Grasemann, G. Laurenczy, *Energy Environ. Sci.* **2012**, *5*, 8171–8181.
[6] F. C. Meunier, *Angew. Chem.* **2011**, *123*, 4139–4140; *Angew. Chem. Int. Ed.* **2011**, *50*, 4053–4054.
[7] D. Preti, C. Resta, S. Squarcialupi, G. Fachinetti, *Angew. Chem.* **2011**, *123*, 12759–12762; *Angew. Chem. Int. Ed.* **2011**, *50*, 12551–12554.
[8] a) C. Hao, S. Wang, M. Li, L. Kang, X. Ma, *Catal. Today* **2011**, *160*, 184–190; b) Y. Yu, J. Fei, Y. Zhang, X. Zheng, *J. Fuel Chem. Technol.* **2006**, *34*, 700–705.

[9] P. G. Jessop, F. Joó, C.-C. Tai, *Coord. Chem. Rev.* **2004**, *248*, 2425–2442.
[10] C. Federsel, R. Jackstell, M. Beller, *Angew. Chem.* **2010**, *122*, 6392–6395; *Angew. Chem. Int. Ed.* **2010**, *49*, 6254–6257.
[11] a) P. G. Jessop, *The Handbook of Heterogeneous Hydrogenation, Homogeneous Hydrogenation of Carbon Dioxide, Part III* (Eds.: J. G. de Vries, C. J. Elsevier), Wiley-VCH, Weinheim, **2008**, Chapter 17; b) W. Leitner, *Angew. Chem.* **1995**, *107*, 2391–2405; *Angew. Chem. Int. Ed. Engl.* **1995**, *34*, 2207–2221.
[12] S. Riduan, Y. Zhang, J. Ying, *Angew. Chem.* **2009**, *121*, 3372–3375; *Angew. Chem. Int. Ed.* **2009**, *48*, 3322–3325.
[13] a) A. Boddien, B. Loges, H. Junge, M. Beller, *ChemSusChem* **2008**, *1*, 751–758; b) S. Enthaler, *ChemSusChem* **2008**, *1*, 801–804; c) T. C. Johnson, D. J. Morris, M. Wills, *Chem. Soc. Rev.* **2010**, *39*, 81–88.
[14] W. Wang, S. Wang, X. Ma, J. Gong, *Chem. Soc. Rev.* **2011**, *40*, 3703–3727.
[15] Y. Inoue, H. Izumida, Y. Sasaki, H. Hashimoto, *Chem. Lett.* **1976**, 863–864.
[16] a) E. Graf, W. Leitner, *J. Chem. Soc. Chem. Commun.* **1992**, 623–624; b) F. Gassner, W. Leitner, *J. Chem. Soc. Chem. Commun.* **1993**, 1465–1466.
[17] a) P. G. Jessop, T. Ikariya, R. Noyori, *Nature* **1994**, *368*, 231–233; b) P. G. Jessop, Y. Hsiao, T. Ikariya, R. Noyori, *J. Am. Chem. Soc.* **1996**, *118*, 344–355.
[18] P. Munshi, A. D. Main, J. C. Linehan, C.-C. Tai, P. G. Jessop, *J. Am. Chem. Soc.* **2002**, *124*, 7963–7971.
[19] a) Y. Himeda, N. Onozawa-Komatsuzaki, H. Sugihara, K. Kasuga, *Organometallics* **2007**, *26*, 702–712; b) T. J. Schmeier, G. E. Dobereiner, R. H. Crabtree, N. Hazari, *J. Am. Chem. Soc.* **2011**, *133*, 9274–9277; c) A. Azua, S. Sanz, E. Peris, *Chem. Eur. J.* **2011**, *17*, 3963–3967.
[20] R. Tanaka, M. Yamashita, K. Nozaki, *J. Am. Chem. Soc.* **2009**, *131*, 14168–14169.
[21] a) Y. Maenaka, T. Suenobu, S. Fukuzumi, *Energy Environ. Sci.* **2012**, *5*, 7360–7367; b) J. F. Hull, Y. Himeda, W.-H. Wang, B. Hashiguchi, R. Periana, D. J. Szalda, J. T. Muckerman, E. Fujita, *Nat. Chem.* **2012**, *4*, 383–388.
[22] R. Langer, Y. Diskin-Posner, G. Leitus, L. J. W. Shimon, Y. Ben-David, D. Milstein, *Angew. Chem.* **2011**, *123*, 10122–10126; *Angew. Chem. Int. Ed.* **2011**, *50*, 9948 –9952.
[23] a) W. R. Thiel, M. Angstl, T. Priermeier, *Chem. Ber.* **1994**, *127*, 2373–2377; b) W. R. Thiel, J. Eppinger, *Chem. Eur. J.* **1997**, *3*, 696–705; c) A. Hroch, G. Gemmecker, W. R. Thiel, *Eur. J. Inorg. Chem.* **2000**, 1107–1114; d) D. Zabel, A. Schubert, G. Wolmershäuser, R. L. Jones, Jr., W. R. Thiel, *Eur. J. Inorg. Chem.* **2008**, 3648–3654; e) K. Muller, A. Schubert, T. Jozak, A. Ahrens-Botzong, V. Schünemann, W. R. Thiel, *ChemCatChem* **2011**, *3*, 887–892; f) L. Taghizadeh Ghoochany, S. Farsadpour, Y. Sun, W. R. Thiel, *Eur. J. Inorg. Chem.* **2011**, 3431–3437.
[24] E. Orselli, G. S. Kottas, A. E. Konradsson, P. Coppo, R. Fröhlich, L. De Cola, A. van Dijken, M. Büchel, H. Börner, *Inorg. Chem.* **2007**, *46*, 11082–11093.
[25] J. Roppe, N. D. Smith, D. Huang, L. Tehrani, B. Wang, J. Anderson, J. Brodkin, J. Chung, X. Jiang, C. King, B. Munoz, M. A. Varney, P. Prasit, N. D. P. Cosford, *J. Med. Chem.* **2004**, *47*, 4645–4648.
[26] V. Vetokhina, K. Dobek, M. Kijak, I. I. Kamińska, K. Muller, W. R. Thiel, J. Waluk, J. Herbich, *ChemPhysChem*, **2012**, *13*, 3661–3671.
[27] a) Z. Zhang, S. Hu, J. Song, W. Li, G. Yang, B. Han, *ChemSusChem* **2009**, *2*, 234–238; b) J. Karl, A. Hank, BASF SE, Ludwigshafen, **2007**, WO 2006/021411 A1, EP1784375 B1.
[28] a) T.-T. Thai, B. Therrien, G. Süss-Fink, *J. Organomet. Chem.* **2009**, *694*, 3973–3981; b) R. Tanaka, M. Yamashita, L. W. Chung, K. Morokuma, K. Nozaki, *Organometallics* **2011**, *30*, 6742–6750.
[29] Y.-Y. Ohnishi, T. Matsunaga, Y. Nakao, H. Sato, S. Sakaki, *J. Am. Chem. Soc.* **2005**, *127*, 4021–4032.
[30] T. Stephenson, G. Wilkinson, *J. Inorg. Nucl. Chem.* **1966**, *28*, 945–956.
[31] a) R. A. Jones, G. Wilkinson, I. J. Colquohoun, W. McFarlane, A. M. R. Galas, M. B. Hursthouse, *J. Chem. Soc. Dalton Trans.* **1980**, 2480–2487; b) R. A. Jones, F. M. Real, G. Wilkinson, A. M. R. Galas, M. B. Hursthouse, K. M. A. Malik, *J. Chem. Soc. Dalton Trans.* **1980**, 511–518.
[32] A. Altomare, G. Cascarano, C. Giacovazzo, A. Guagliardi, M. C. Burla, G. Polidori, M. Camalli, *J. Appl. Crystallogr.* **1994**, *27*, 435–435.
[33] G. M. Sheldrick, *Acta Crystallogr. Sect. A* **2008**, *64*, 112–122.
[34] a) *CrysAlisPro, Version 1.171.33.48*, Oxford Diffraction Ltd, Oxford, **2009**; b) *CrysAlisPro, Version 1.171.33.66*, Oxford Diffraction Ltd, Oxford, **2010**.
[35] a) P. J. Stephens, F. J. Devlin, C. F. Chabalowski, M. J. Frisch, *J. Phys. Chem.* **1994**, *98*, 11623–11627; b) A. D. Becke, *J. Chem. Phys.* **1993**, *98*, 5648–5652; c) A. D. Becke, *Phys. Rev. A* **1988**, *38*, 3098–3100; d) C. Lee, W. Yang, R. G. Parr, *Phys. Rev. B* **1988**, *37*, 785–789.
[36] a) A. Schäfer, C. Huber, R. Ahlrichs, *J. Chem. Phys.* **1994**, *100*, 5829–5835; b) K. Eichkorn, F. Weigend, O. Treutler, R. Ahlrichs, *Theor. Chem. Acc.* **1997**, *97*, 119–124.
[37] D. Andrae, U. Häußermann, M. Dolg, H. Stoll, H. Preuß, *Theor. Chim. Acta* **1990**, *77*, 123–141.
[38] F. Weigend, R. Ahlrichs, *Phys. Chem. Chem. Phys.* **2005**, *7*, 3297–3305.
[39] *TURBOMOLE, V6.4 2012*, a development of University of Karlsruhe and Forschungszentrum Karlsruhe GmbH, 1989–2007, TURBOMOLE GmbH, since 2007; available from http://www.turbomole.com.
[40] Gaussian 03, Revision C.02, M. J. Frisch, G. W. Trucks, H. B. Schlegel, G. E. Scuseria, M. A. Robb, J. R. Cheeseman, J. A. Montgomery, Jr., T. Vreven, K. N. Kudin, J. C. Burant, J. M. Millam, S. S. Iyengar, J. Tomasi, V. Barone, B. Mennucci, M. Cossi, G. Scalmani, N. Rega, G. A. Petersson, H. Nakatsuji, M. Hada, M. Ehara, K. Toyota, R. Fukuda, J. Hasegawa, M. Ishida, T. Nakajima, Y. Honda, O. Kitao, H. Nakai, M. Klene, X. Li, J. E. Knox, H. P. Hratchian, J. B. Cross, V. Bakken, C. Adamo, J. Jaramillo, R. Gomperts, R. E. Stratmann, O. Yazyev, A. J. Austin, R. Cammi, C. Pomelli, J. W. Ochterski, P. Y. Ayala, K. Morokuma, G. A. Voth, P. Salvador, J. J. Dannenberg, V. G. Zakrzewski, S. Dapprich, A. D. Daniels, M. C. Strain, O. Farkas, D. K. Malick, A. D. Rabuck, K. Raghavachari, J. B. Foresman, J. V. Ortiz, Q. Cui, A. G. Baboul, S. Clifford, J. Cioslowski, B. B. Stefanov, G. Liu, A. Liashenko, P. Piskorz, I. Komaromi, R. L. Martin, D. J. Fox, T. Keith, M. A. Al-Laham, C. Y. Peng, A. Nanayakkara, M. Challacombe, P. M. W. Gill, B. Johnson, W. Chen, M. W. Wong, C. Gonzalez, J. A. Pople, Gaussian, Inc., Wallingford CT, **2004**.
[41] Gaussian 09, Revision B.1, M. J. Frisch, G. W. Trucks, H. B. Schlegel, G. E. Scuseria, M. A. Robb, J. R. Cheeseman, G. Scalmani, V. Barone, B. Mennucci, G. A. Petersson, H. Nakatsuji, M. Caricato, X. Li, H. P. Hratchian, A. F. Izmaylov, J. Bloino, G. Zheng, J. L. Sonnenberg, M. Hada, M. Ehara, K. Toyota, R. Fukuda, J. Hasegawa, M. Ishida, T. Nakajima, Y. Honda, O. Kitao, H. Nakai, T. Vreven, J. A. Montgomery, Jr., J. E. Peralta, F. Ogliaro, M. Bearpark, J. J. Heyd, E. Brothers, K. N. Kudin, V. N. Staroverov, R. Kobayashi, J. Normand, K. Raghavachari, A. Rendell, J. C. Burant, S. S. Iyengar, J. Tomasi, M. Cossi, N. Rega, J. M. Millam, M. Klene, J. E. Knox, J. B. Cross, V. Bakken, C. Adamo, J. Jaramillo, R. Gomperts, R. E. Stratmann, O. Yazyev, A. J. Austin, R. Cammi, C. Pomelli, J. W. Ochterski, R. L. Martin, K. Morokuma, V. G. Zakrzewski, G. A. Voth, P. Salvador, J. J. Dannenberg, S. Dapprich, A. D. Daniels, Ö. Farkas, J. B. Foresman, J. V. Ortiz, J. Cioslowski, D. J. Fox, Gaussian, Inc., Wallingford CT, **2009**.
[42] A. Klamt, G. Schüürmann, *J. Chem. Soc. Perkin Trans. 2* **1993**, 799–805.
[43] Y. Zhang, J. Yang, Y.-X. Yu, *J. Phys. Chem. B* **2005**, *109*, 13375–13382.

Received: November 23, 2012
Revised: February 19, 2013
Published online: April 15, 2013

